I.O.S.

THE EFFECT OF TURBULENCE ON THE CALIBRATION OF ELECTROMAGNETIC CURRENT SENSORS AND AN APPROXIMATION OF THEIR SPATIAL RESPONSE

by
G GRIFFITHS

REPORT NO. 68

1979

NATURAL ENVIRONMENT RESEARCH COUNCIL

INSTITUTE OF OCEANOGRAPHIC SCIENCES

INSTITUTE OF OCEANOGRAPHIC SCIENCES

Wormley, Godalming,
Surrey, GU8 5UB.
(0428 - 79 - 4141)

(Director: Dr. A.S. Laughton)

Bidston Observatory,
Birkenhead,
Merseyside, L43 7RA.
(051 - 653 - 8633)

(Assistant Director: Dr. D.E. Cartwright)

Crossway,
Taunton,
Somerset, TA1 2DW.
(0823 - 86211)

(Assistant Director: M.J. Tucker

THE EFFECT OF TURBULENCE ON THE CALIBRATION OF ELECTROMAGNETIC CURRENT SENSORS AND AN APPROXIMATION OF THEIR SPATIAL RESPONSE

G. GRIFFITHS

REPORT NO. 68

1979

Institute of Oceanographic Sciences,
Wormley, Godalming, Surrey GU8 5UB.

CONTENTS

List of Symbols

b	wake width parameter (mixing length theory)
B	magnetic flux density
Cd	cylinder drag coefficient
d	diameter of cylinder
fv	Strouhal frequency
L	sensor averaging length
R	Reynolds number
St	Strouhal number
u	fluctuation velocity in x direction
u_1max	maximum velocity deficit at the centre of the wake
$\overline{uv}$	time averaged uv velocity fluctuation covariance
u_1av	velocity deficit measured by sensor
u_1	velocity deficit in the wake
U_∞	free stream velocity
U_1	velocity within the wake
v	fluctuation velocities in y direction
V	velocity field
w	fluctuation velocities in z direction
x	distance downstream of sensor from cylinder
y	distance from centre axis of the wake
β	mixing length constant
ε_o	parameter for shear stress hypothesis
η	wake width parameter (shear stress hypothesis)

Introduction

1.0 EM Current Sensors in Turbulent Flow

Electromagnetic current sensors are being used increasingly in situations where the interest is in fluctuations in the flow as well as in the mean flow. Examples of these uses are Reynolds stress measurements in the bottom boundary layer, and near the surface.

A sensor having perfect response to a steady laminar flow may not have a perfect response to mean flow in turbulent conditions. Further, due to spatial averaging the output of the sensor indicating flow fluctuations may not represent the true turbulence. Electromagnetic current sensors are fundamentally integrating sensors; the output being a weighted integral of $B \times V$ in the neighbourhood of the coil. Thus it is reasonable to assume that any EM sensor will have a limit to its spatial resolution, which may be of the order of the coil diameter, or the electrode separation. As far as is known no analysis has been made of this.

This report attempts to describe the response of four electromagnetic current sensors to a partly turbulent stream of known characteristics, and from this, to deduce the spatial response of the sensors. The response in laminar flow has been described in Griffiths, Collar and Braithwaite (1978).

The four EM sensors subjected to turbulence were:

(a) an 11.1 cm diameter discus sensor, manufactured by Colnbrook Instrument Development Ltd* under licence from IOS;

(b) an experimental miniature discus sensor of 5 cm diameter, made by C.I.D.;

(c) a development version of the IOS annular EM sensor, of diameter 16 cm;

(d) an experimental spherical sensor with electrodes protruding 1 cm from the surface, of diameter 13.4 cm, made at IOS.

---

*Colnbrook Instrument Development Ltd, Poyle Road, Colnbrook, Bucks SL3 0AJ.

Of the several possible ways of generating turbulence in a towing tank, the method chosen was to tow a rigid cylinder of diameter 2 cm to 5 cm many diameters upstream of the sensor. The cylinder length was such that the angle between the sensor and the surface and the lower end of the cylinder was about 20^{o}, compared to the wake angle of $\sim 4^{o}$, Fig. 1.

Theoretical descriptions of the wake of a cylinder were made by Prandtl (1953) and developed by Schlichting (1955) and Hinze (1959). Together with the results of Townsend (1947, 1949), these enabled us to calculate the expected mean flow, flow fluctuations and $\overline{uv}$ covariance as a function of the x and y position within the wake. The work of Townsend (1947, 1949) was carried out in wind tunnels, at similar Reynolds numbers to those used in this series of experiments, and largely confirm the validity of the later theories.

In order to keep the Reynolds number close to that used by Townsend, the flow velocity was kept within the range of 15 cm/sec to 23 cm/sec. The sensor outputs were limited to 3 Hz (-3 dB) before sampling, and from the expression $\lambda = c/f$, with c_{min} at 15 cm/sec and f_{max} at 3 Hz, the minimum length scale of fluctuations that could be observed was 5 cm. The cylinder diameter was chosen to maximize flow fluctuations, but not to cause a blocking effect by exceeding 4% of the width of the tank. As the experiments required the sensor to be many diameters downstream of the cylinder, this set an upper limit to the diameter of the cylinder because of the towing tank carriage length. Underlying the choice of mean flow speed and cylinder diameter was the need to keep the relation of root mean square velocity fluctuations to mean flow similar to that found in some oceanic situations (Heathershaw, 1975, Thorpe, Collins and Gaunt, 1973, Bowden and Fairbairn, 1956), and in most of the experiments the ratio was about 1:14.

The experiments made and their purpose are as follows:

1. Measurement of the mean flow in the centre of the wake as a function of distance behind the cylinder. This was to show the response of an EM sensor to turbulent flow, and to obtain an approximate averaging length (Section 3.1).

2. Measurement of the velocity profile across the width of the wake, with fluctuation velocities and covariance. The aim was to show the ability of the sensors to measure fluctuations (Sections 3.3 and 3.4).

3. Resolution of the Kármán vortex sheet near the cylinder to show the ability of the sensors to indicate small scale flow variations (Section 4).

4. Measurements of wave orbital velocities for waves of varying wavelength, achieved by Doppler shift between a moving sensor and a constant frequency wave. The aim was to find the spatial response from a 'single frequency' measurement (Section 5).

An attempt was made to indicate the spatial response from a spectral analysis of the measurements at the centre of the cylinder wake. The output spectrum should be that of the wake turbulence modified by the transfer function of the sensor. This experiment failed to give consistent results because of the uncertainty over the input spectrum, and the lack of a standard instrument for its measurement.

2.0 Flow behind a cylinder

The usual method of creating laboratory wind tunnel turbulence is by a grid, while Olsen (1936) successfully used a row of rods. However, it was felt that their use in a towing tank would be difficult due mainly to the blocking effect, and hence uncertainty in the true mean flow at the sensor. The work of Townsend (1947) suggested the use of a single cylinder to generate turbulence. As the distance downstream from the cylinder increases, the vortex sheet decays to turbulence, the process starts at $^{x}/d \sim 25$, but is not completed until $^{x}/d > 500$. Practical limits set by the maximum separation available on the carriage meant that $^{x}/d \leq 65$ for

most of the experiments in this report.

Corrections to the mean flow need to be considered due to the finite dimensions of the towing tank. Pankhurst and Holder (1952) give a full account of solid and wake blockage for a cylinder in a wind tunnel. The solid blockage, of the order $(d/Q)^2$, where Q is the tank width, amounts to 0.06% of the mean flow. Wake blockage is more important, the correction $\frac{1}{4}.\frac{d}{Q}.Cd$ amounts to 0.6%. This can be neglected as it is below the sensor noise level. The effect on the wake profile at the sensor, however, may be larger, but we think it unlikely to cause errors exceeding ±2 mm/sec (1.3% of mean flow), the uncertainty in sensor zero velocity output and tank circulation currents.

2.1 Mean flow calculation

Approximate expressions given in Schlichting (1955) for the mean velocity profile behind a cylinder in a flowing fluid of finite extent increase in validity as the ratio x/d increases. Using the mixing length theory of Prandtl, Schlichting obtains:

$$\frac{u_1}{U_\infty} = \frac{\sqrt{10}}{18\beta}.\left(\frac{x}{Cd.d}\right)^{-\frac{1}{2}} \qquad (1) \text{ at } y = 0$$

where β is a wake width parameter of the mixing length theory determined on the basis of measured values. For $x/d < 50$ additional terms in x^{-1} and $x^{-3/2}$ should be included. Using the shearing stress hypothesis, Schlichting (1955) gives:

$$\frac{u_1}{U_\infty} = \frac{1}{4\sqrt{\pi}}.\sqrt{\frac{1}{.0222}}.\left(\frac{x}{Cd.d}\right)^{-\frac{1}{2}} \qquad (2) \text{ for } x/d > 50$$

Subsequent calculations assume the drag coefficient of the cylinder to be constant at approximately 1 over the range of Reynolds number used.

Both of these expressions can be reduced to the forms plotted in Fig. 2:

$$\frac{u_1}{U_\infty} = \frac{k}{\sqrt{x}} \qquad (3) \text{ where } k = 2.14 \text{ mixing length}$$

$$k = 2.07 \text{ shear stress}$$

for d = 4.8 cm.

The y profiles from the two hypotheses give

$$\frac{u_1}{u_1 max} = \left(1 - \left(\frac{y}{b}\right)^{3/2}\right)^2 \qquad (4) \text{ where } b = \frac{1}{x}(x.Cd.d)^{\frac{1}{2}},$$

which is shown in Fig. 3, a measure of the wake width.

and from the shear stress:

$$\frac{u_1}{u_1 max} = \exp\left(-1/4\eta^2\right) \qquad (5) \text{ where } \eta = y\frac{u_o}{\varepsilon_o x}$$

$$\text{and } \varepsilon_o = .0222\ U\infty.Cd.d$$

from Schlichting (1955).

These velocity profiles are valid only for point velocity sensors, such as hot wire devices; the electromagnetic sensors, with larger integrating volumes, produce an average of the profile. The above expressions were averaged over the length of the electrode path to give a first approximation to the integration performed by the sensor. As the profile changes slowly with averaging length, the comparison of the theoretical profile with the observations cannot be used as an accurate indicator of the averaging length. Appendix 1 derives a form of equation 4 for use when the profile is averaged when the sensor remains on the axis y = 0.

2.2 Flow fluctuations

Townsend (1947) and Tritton (1977) give experimental results (Fig. 4) for the fluctuations of the three components u,v, and w within the wake of a cylinder and also for the covariance $\overline{uv}$. As these results were obtained at a large ratio of $^x/d$ (from 90), exact comparison with our results at $^x/d < 75$ must not be expected.

3.0 Experimental Results

The 11 cm and 5 cm diameter discus sensors were used in conjunction with a 2 cm diameter cylinder at $^x/d \lesssim 75$, while the spherical sensor and the annulus were tested with a 4.8 cm diameter cylinder. In the initial experiments, 200 point data sets sampled at 10 Hz were taken; later experiments were made using the CAMAC/PDP-11 laboratory system, with 1000 point data sets sampled at 20 Hz.

Following the averaging hypothesis set out in section 2.1 the measured profiles were compared with those obtained from the theoretical profiles averaged over a length corresponding to the electrode separation.

3.1 X-axis velocity profile

3.1.1 11 cm and 5 cm discus

The experimental results for these two sensors show close agreement with the averaged theoretical profile for the mean flow; the maximum error being -4% for the 5 cm sensor (Fig. 5). Experimental error arising from known causes was ±2%. The errors due to the uncertain averaging length and the inapplicability of the theory at $^{x}/d < 100$ are unknown. However, any changes in calibration of the sensors due to turbulent flow were thus less than 4% of the mean flow.

3.1.2 Annular sensor

The discrepancy between the theoretical and observed profiles for the annulus cannot be explained by known experimental errors. Experiments based on much larger samples of 5000 points were unable to reduce the discrepancy significantly (Fig. 6). All the measurements suggest that the annulus has an integrating length of less than the electrode separation. It is known that the velocity field within the annulus is not uniform (Griffiths, Collar and Braithwaite (1978)) and the discrepancy may arise from this.

3.2 Y-axis velocity profile

The mean flow in the y-direction within the wake of a cylinder is small, typically 2% of the mean x axis flow from Townsend (1949). This is of the order of the errors in this experiment (±1%) and hence the results should be treated with caution. Note the difference in the behaviour of the spherical and annular sensors (Fig. 7). The peak $\overline{v}$ flow for the sphere was at the centre of the wake, 9 mm/sec, and from y = 3 cm to y = 20 cm, the mean flow was ~4 mm/sec. The annulus results seem closer to the expected form, with a flow of ~±2 mm/sec near the centre and edge of the wake, and a flow of ~4 mm/sec from y = 8 cm to y = 16 cm.

3.3 X-axis velocity as a function of y-axis function

These profiles are of interest as they indicate clearly the averaging properties of the e.m. sensors, and because of the presence of strong shear (up to 12 cm/sec/metre) within the averaging volume of the sensor.

3.3.1 11 cm and 5 cm discus

The 11 cm discus gave results in close agreement with the expected profile averaging over 8 cm (Fig. 8a). Errors were within ±3% for the 11 cm discus, and ±4% for the 5 cm discus. The graphs show clearly the effect of the difference in electrode path averaging between the two sensors (Fig. 8b). The noise level of the 5 cm sensor was higher than that of the 11 cm discus.

3.3.2 Spherical sensor

The mean flow measured by the sphere was close to the expected result (Fig. 9), with deviations of ±3% although the errors seem systematic. Within the wake, the noise level was little changed from that outside.

3.3.3 Annulus

With the interest shown in measuring turbulent fluctuations with this sensor, a more detailed experiment was made by logging multiple 1000 point data sets using a CAMAC/PDP-11 system. This enabled estimates of repeatability to be made. In the 200 sample data sets, deviations were a maximum of ±3%, based on a sensor averaging length of 10 cm. Increasing the number of samples to 5000 reduced the errors to +2%, -1.5% (Fig. 10) with uncertainty in zero output and tank circulating currents amounting to ±1%. Statistical uncertainty of the true mean amounted to ±0.5%. As the form of the errors remained approximately consistent between the sets of data, a systematic error cannot be excluded but if present, this must be below ±2%.

3.4 Turbulent Fluctuation Velocities within the Wake

Griffiths, Collar and Braithwaite (1978) discuss noise in electromagnetic current sensors, and the effect of the design upon sensor noise level. In

this series of experiments the mean square turbulent velocities were several times greater than the levels at rest and in laminar flow. However, over the band 0.1 Hz to 5 Hz, the ratio of turbulence 'noise' to instrumental noise changed, and a graph is given in Fig. 11.

When examining the fluctuation velocities, some filtering was carried out to remove spikes from the data. This took the form of removing any data points showing a rate of change greater than 40 cm/sec^2.

In the graphs of sensor noise levels, the y ordinate is plotted in terms of a normalized quantity:

$$\frac{\overline{U^2}(x - x_o)}{U_\infty^2 \, d}$$ Tritton (1977)

which enables comparisons to be made for different U_∞, x and d.

Both discus sensors, Fig. 12, showed a low fluctuation power to sensor noise ratio. Apart from a trend towards increased $\overline{U^2}$ at the wake centre, the experiment was not able to produce a reliable fluctuation velocity profile. The annular sensor with its higher fluctuation to noise ratio achieved produced a velocity profile (Fig. 13b) similar to that described in Tritton (1977). The $\overline{v^2}$ profile (Fig. 13b) showed a trend towards extension of the wake edge. Less confidence can be placed in the results for the sphere (Fig. 14) because of the lower ratio of fluctuation velocity to noise level but the trend was toward increased noise at the wake centre.

Another test of the ability of the sensors to resolve the flow fluctuations correctly is the covariance $\overline{uv}$ across the wake, and the derived correlation coefficient $r_{uv} = \overline{uv}/(\overline{U^2}.\overline{V^2})^{\frac{1}{2}}$. A curve similar to that in Tritton (1977) was obtained for the annulus (Fig. 15a), averaging over 200 samples. The results for the sphere (Fig. 15b) did not converge within 200 samples and it is doubtful if the sphere was able to resolve correctly the uv fluctuations within the passband 0.1 to 3 Hz. As the 11 cm and 5 cm discus were used together on this experiment, the limited number of data channels available meant we were unable to obtain $\overline{uv}$ correlations for these sensors.

The results for the annular and 11 cm discus sensors are different to those expected from measurements in laminar flow by Griffiths, Collar and Braithwaite (1978) in that both sensors showed a good signal to noise ratio for the aligned axis flow. In turbulent flow, the annulus follows the expected form, but the discus gave a low fluctuation output across the wake. This may be due to suppression of the w components of the turbulence similar to the stalling in mean W flow detailed in Griffiths, Collar and Braithwaite (1978).

4.0 The response of the discus sensor to a Kármán vortex sheet behind a long cylinder

At small ratios of $^{x}/d$, from 10 to 20, the wake of a cylinder exhibits periodic shedding of vortices before the wake becomes turbulent.

The frequency of the vortex shedding can be calculated from a knowledge of the Strouhal number. Over the range of Reynolds number 10^3 to 10^5 this can be approximated by St = 0.2 (factors such as surface roughness affect the value of St).

Then $St \sim \frac{fv.d}{U_\infty}$

fv = frequency of vortex shedding

d = cylinder diameter

U_∞ = velocity.

Experiments were carried out using the 11 cm diameter discus behind a 4.8 cm diameter cylinder at a speed of approximately 15 cm/sec. At $^{x}/d = 12.5$, the striking features on the UV recorder output (Fig. 16a) was the Strouhal frequency component. A simple spectral analysis (Fig. 17a) showed the peak to be at 0.53 Hz compared with the calculated 0.6 Hz. The spectrum showed very little energy above 1 Hz, indicating that turbulence had not developed. Energy on the transverse axis was mainly at the Strouhal frequency, with less than 1% of the total energy lying above 0.75 Hz.

Increasing $^{x}/d$ to 34 reduced the peak around the Strouhal frequency, but the origin of most of the fluctuations was still the vortex shedding, with some turbulent mixing taking place (Figs. 16b and 17b). On the axis

transverse to the flow the turbulence had developed and considerable energy was found up to 5 Hz, the Nyquist frequency. At $^{x}/d = 75$, achieved by changing to a 2 cm cylinder, no well defined peak was seen at the Strouhal frequency of 2.1 Hz. This leads to the conclusion that at such values of $^{x}/d$, the turbulence is fairly well developed, Townsend (1947) works from $^{x}/d = 80$, but suggests a lack of self-preservation until $^{x}/d \geq 500$.

5.0 Spatial Response of the annular sensor as derived from measurements in waves

The aim of the experiment was to find the response of the toroid sensor to wave orbital velocities for waves of different horizontal wavenumbers. In order to achieve this, it was desired to make measurements with wavelengths of 10 cm to over 100 cm. The method chosen was to use a fixed frequency wave-train, and to shorten or lengthen the apparent wavelength seen at the sensor by the use of Doppler shift between the moving carriage and the stationary wavemaker (Fig. 18). Using wavemaker frequencies of 0.5 Hz and 0.6 Hz, and carriage speeds of 90 cm/sec and less, a wavelength range of 26 cm to 126 cm was obtained. This was the limit due to wavemaker restrictions, and the contamination of the data by hydrodynamic noise generated by the sensor supports at the higher speeds. This noise meant it was impracticable to use this method for the spherical sensor or for the discus sensor in a horizontal mode.

Clearly, Fig. 19a suggests that the sensor has a uniform amplitude response to 50 cm, and then a slow decrease. Assuming the response is of the form $\sin(\pi L/\lambda)/(\pi L/\lambda)$, a least squares fit was made between the data set and the calculated $\sin(\pi L/\lambda)/(\pi L/\lambda)$ based on averaging lengths of 2 cm to 16 cm, Fig. 19b. A minimum in the squared residuals was found at $L = 9 \text{ cm } ^{+ 1.5 \text{ cm}}_{- 2.5 \text{ cm}}$ at +30% limits. A spectrum computed and averaged from 200 samples (Fig. 19c) shows the unambiguous wave frequency.

6.0 Conclusions

The effects of turbulence on the calibration of current sensors has not been widely discussed, but the report by Bivins and Appell (1976) showed

a cylindrical e.m. sensor to have a large error in mean flow measurement in the presence of grid generated turbulence.

In order to compare the experimental results to a simple theory, the turbulence used in our experiments was generated by a single rigid cylinder. This enabled calculations of mean flow, turbulent fluctuations and uv correlations to be made.

The results obtained for the measurement of mean flow had deviations from theory similar to the known experimental errors. Thus in the presence of turbulent fluctuations of the order of 1 cm/sec rms, the sensors showed no significant systematic errors. Measurements were made in regions of strong shear (12 cm/sec/metre) and the mean flow results showed no significant errors.

Flow fluctuation measurements showed larger deviations from the theory, and from the wind tunnel work of Townsend (1947). The measurement of such low level flow fluctuations has inherent problems, in repeatability and because of the sensor noise level, but the results for the annulus agree qualitatively with those of Townsend (1947). For the annulus, the correlations of $\overline{uv}$ were calculated, and compared well with the description of Tritton (1977). A lack of convergence for the spherical sensor $\overline{uv}$ correlations suggests that this sensor did not measure the u,v fluctuations correctly.

The attempt to define the averaging length of the sensor from the wake width measurements merely confirmed the assumption that it is of the order of the electrode separation. As the sensitivity of the method was not high, quantitative results could not be deduced. Limitations associated with the wavemaker, and hydrodynamic noise generated by the sensor supports set a limit to the range of this method for defining the averaging length. Scales down to 25 cm were obtained, and the results showed the annular sensor to have a uniform response to 50 cm, and interpolation assuming a $\sin(\pi L/\lambda)/(\pi L/\lambda)$ form for the spatial response gave the averaging length as 9 cm, compared to an electrode separation of 10 cm.

References

Bivins, L.E. and G.F. Appel (1976) Turbulence effects on current measuring transducers, Exposure 3, (6), 1-5.

Bowden, K.F. and L.A. Fairbairn (1956) Measurements of turbulent fluctuations and Reynolds stresses in a tidal current, Proc. Roy. Soc. (A), 237, 422-438.

Griffiths, G., P.G. Collar and A.C. Braithwaite (1978) Some characteristics of electromagnetic current sensors in laminar flow conditions, IOS Internal Report No. 56.

Heathershaw, A.D. (1975) Measurements of turbulence near the sea-bed using electromagnetic current meters, Proc. IERE Conference on Instrumentation in Oceanography, Bangor, 1975.

Hinze, J.O. (1959) Turbulence, McGraw Hill.

Olsen, R.G. (1936) Geschwindigkeits und Temperaturverteilung hinter einem Gitter bei turbulenter Strömung, Zeitschrift für Angewandte Mathematik und Mechanik, Vol. 16, No. 5, October 1936.

Pankhurst and Holder (1952) Wind Tunnel Technique, Pitman.

Prandtl, L. (1953) Essentials of Fluid Dynamics, Blackie.

Schlichting, H. (1955) Boundary Layer Theory, Pergamon.

Thorpe, S.A., E.P. Collins and D.I. Gaunt (1973) An electromagnetic current meter to measure turbulent fluctuations near the ocean floor, Deep Sea Research, 20, 933-938.

Townsend, A.A. (1947) Measurements in the turbulent wake of a cylinder, Proc. Roy. Soc., Vol. 190, Series A.

Townsend, A.A. (1949) Momentum and energy diffusion in the turbulent wake of a cylinder, Proc. Roy. Soc., Vol. 197, Series A.

Tritton, D.J. (1977) Physical Fluid Dynamics, Van Nostrand Reinhold.

Appendix 1

Procedure for finding the integrated velocity profile over the y axis

The velocity deficit in the x direction as a function of y can be approximated by:

$$u_1 = \left(1 - \left(\frac{y}{b}\right)^{\frac{3}{2}}\right)^2 . u_1max \qquad \text{for } y \leqslant b \qquad (6)$$

and $u_1 = 0 \qquad y \geqslant b.$

Integrating over the limits 0 to b, and dividing by $L/2$ gives u_1av for $L/2 \geqslant b$:

$$\frac{u_1av}{u_1max} = \frac{2}{L}\int_0^{y=b}\left(1 - \left(\frac{y}{b}\right)^{\frac{3}{2}}\right)^2 dy \qquad (7)$$

$$\text{integrating:} \quad = \frac{2}{L}\left(y - \frac{0.8y^{\frac{5}{2}}}{b^{\frac{3}{2}}} + \frac{y^4}{4b^3}\right)_{y=0}^{y=b} \qquad (8)$$

$$\text{substituting:} \quad = \frac{2}{L}(0.45b) \qquad (9)$$

$$\therefore \; u_1av = \frac{0.9b\ u_1max}{L} \qquad (10)$$

In the case where $L/2 \leqslant b$ change the limits in equation (8) to 0 to $L/2$ and hence

$$u_1av = \frac{2}{L}\left(\frac{L}{2} - \frac{0.8L^{\frac{5}{2}}}{2^{\frac{5}{2}}.b^{\frac{3}{2}}} + \frac{L^4}{2^4.4.b^3}\right)u_1max \qquad (11)$$

$$u_1av = \left(1 - \frac{0.283L^{\frac{3}{2}}}{b^{\frac{3}{2}}} + \frac{L^3}{32b^3}\right)u_1max \qquad (12)$$

In principle, these equations could be used to find L from the experimental data.

If $L/2 \geqslant b$ we have, from equation 10:

$$L = \frac{0.9\ u_1max\ b}{u_1av} \qquad (13)$$

Substituting for u_1max from equation 3, and b from equation 4 we have:

$$L = \frac{0.96\sqrt{d}.U_\infty}{u_1av} \qquad (14)$$

Thus, if $b \leqslant L/2$, then the mean output of sensor is independent of x.

Alternatively, if $b >> L/2$, from equation 12:

$$L = \sqrt[\frac{2}{3}]{\frac{b^2(u_1av - u_1max)}{0.283\ u_1max}} \qquad (15)$$

The second method results in larger errors because of the error in forming the small difference $(u_1av - u_1max)$, however, the first method has to be used at very low ratios of x/d, and the Strouhal frequency predominates which makes accurate mean flow measurement difficult.

Appendix 2

The effect of a moving sensor on the apparent wavelength of a fixed frequency wavetrain

If the water depth is much greater than the amplitude of the surface waves, then the wavelength is given by

$$\lambda_o = \frac{g}{2f^2\pi} \quad (1)$$

g = acceleration due to gravity

When the sensor is at rest

$$\lambda_{EMCM} = \lambda_o = \frac{c}{f} \quad (2)$$

c = velocity of propagation

λ_{EMCM} = apparent wavelength at the sensor

f = frequency of the wavemaker

Consider one cycle, the wavelength is altered by an amount V.T' where T' is the period of the apparent wave, when the sensor is moving with velocity V.

Thus $\lambda_{EMCM} = \frac{c}{f} - V.T'$ (3)

but $T' = \frac{1}{f} = \frac{\lambda_{EMCM}}{c}$ (4)

Substitute (4) into (3) $\lambda_{EMCM} = \frac{c}{f} \pm \frac{V\lambda_{EMCM}}{c} = \frac{c}{f(1 + \frac{V}{c})}$ (5)

For example, with the wavemaker set at 0.75 sec period, velocities of up to ±60 cm/sec would produce a range of 88 cm λ at rest to 180 cm wavelength moving away from the wavemaker and 58 cm wavelength moving toward the source. Reducing the wave period to 0.5 s enabled us to reach apparent wavelengths of 25 cm.

Throughout the experiment the depth of the sensor was kept constant, and as the wave orbital velocities depend only on the wavemaker period, there was no change of these velocities with apparent wavelength.

List of Figures

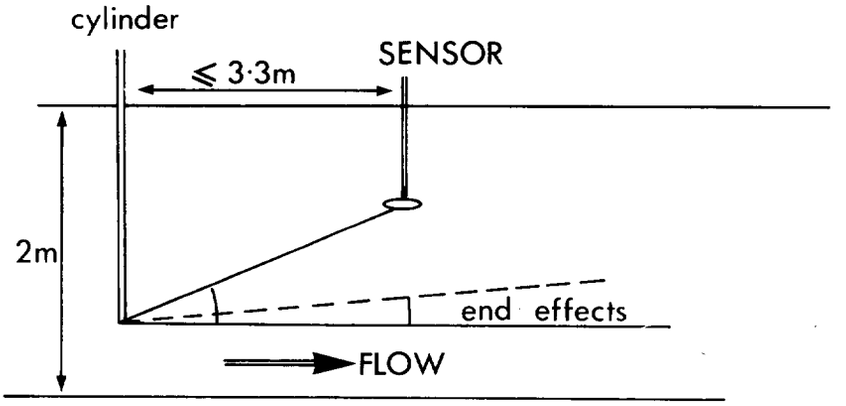

Figure 1. Towed cylinder and sensor arrangement in the towing tank.

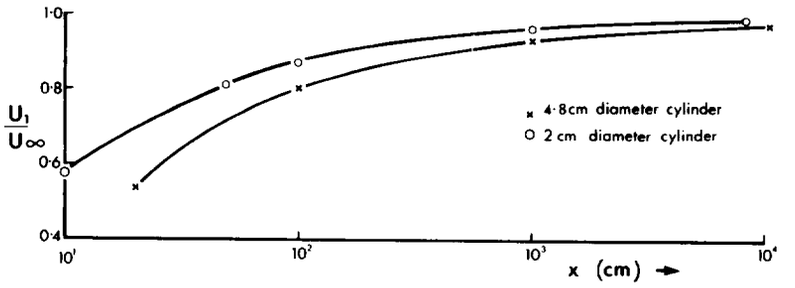

Figure 2. Mean flow behind a towed cylinder.

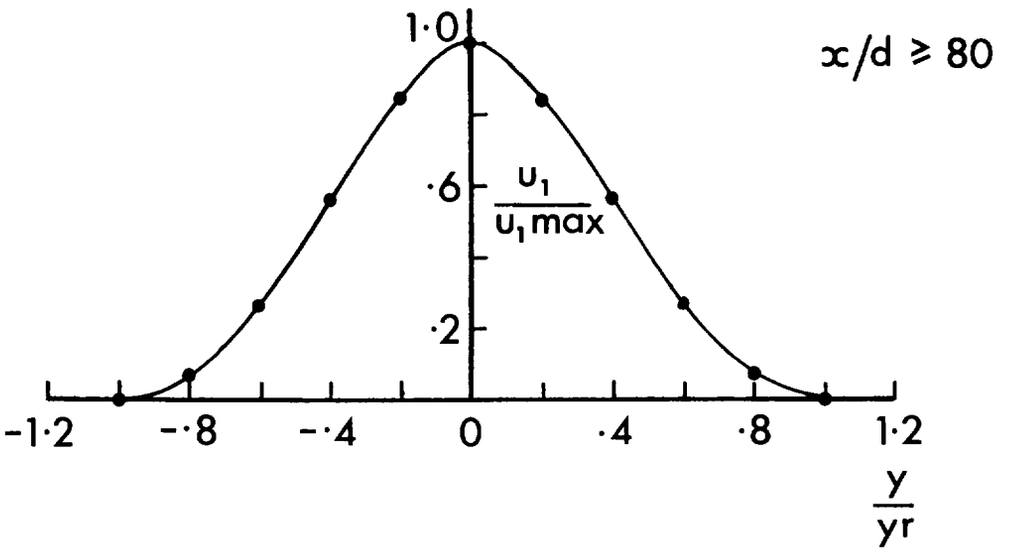

Figure 3. Velocity distribution in a two dimensional wake behind a cylinder.

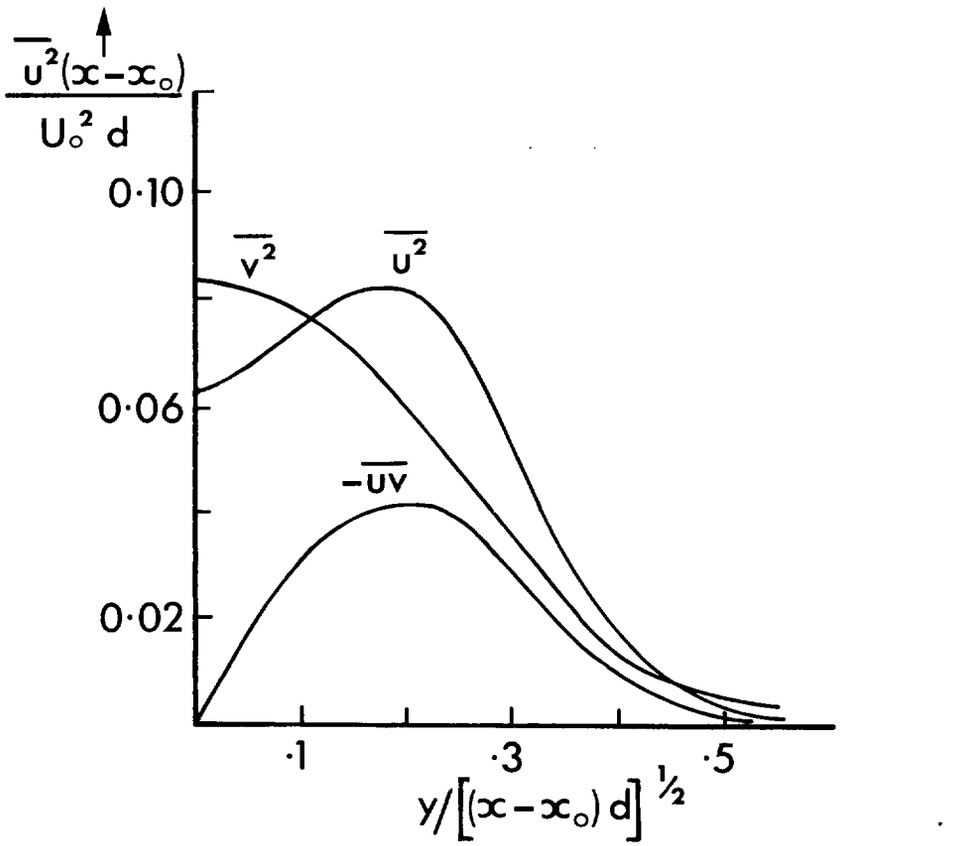

Figure 4. Velocity fluctuation and correlation in a two dimensional wake (from Tritton (1977)).

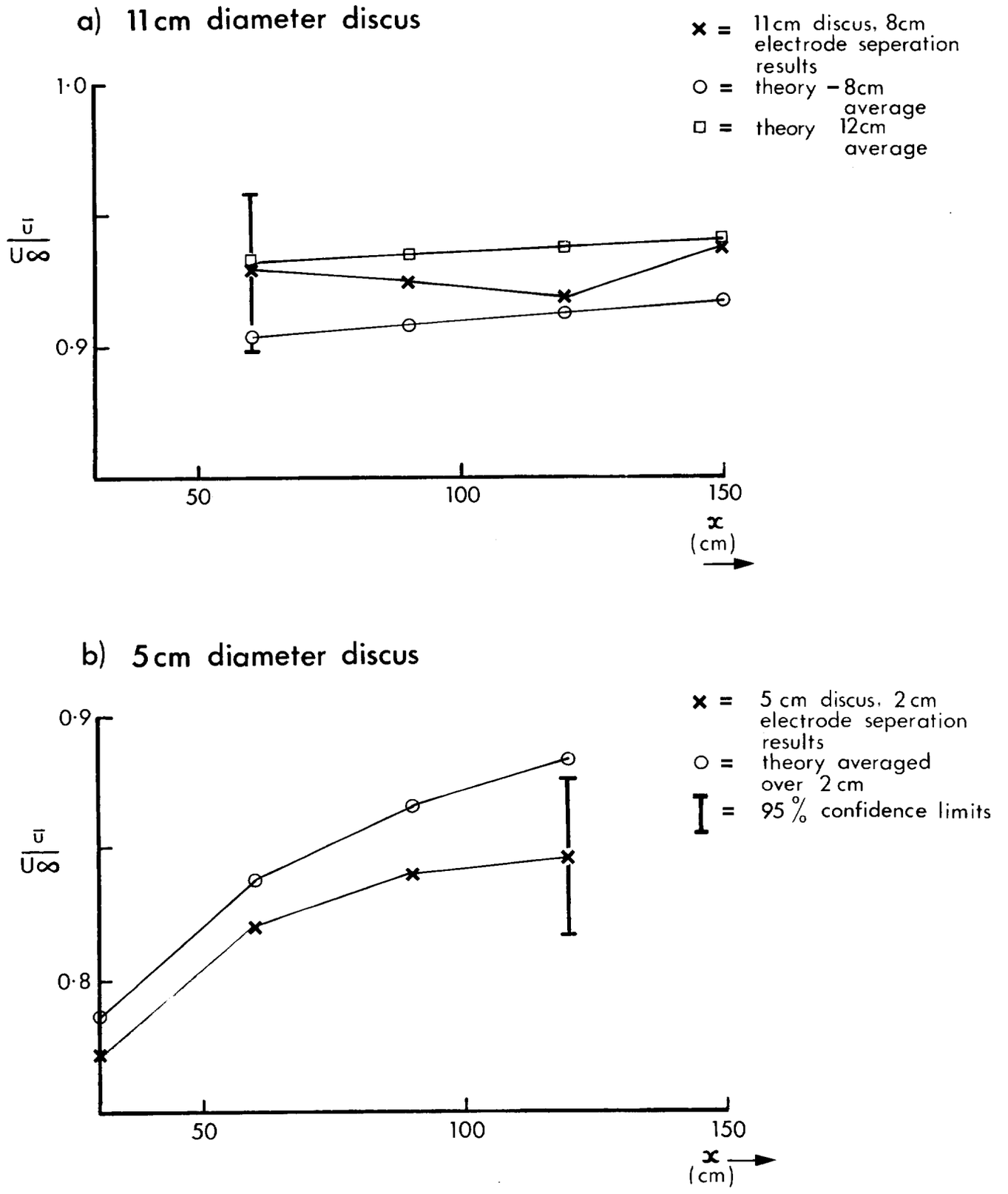

Figure 5. X axis velocity measured by discus sensors in the wake of a 2 cm diameter cylinder.

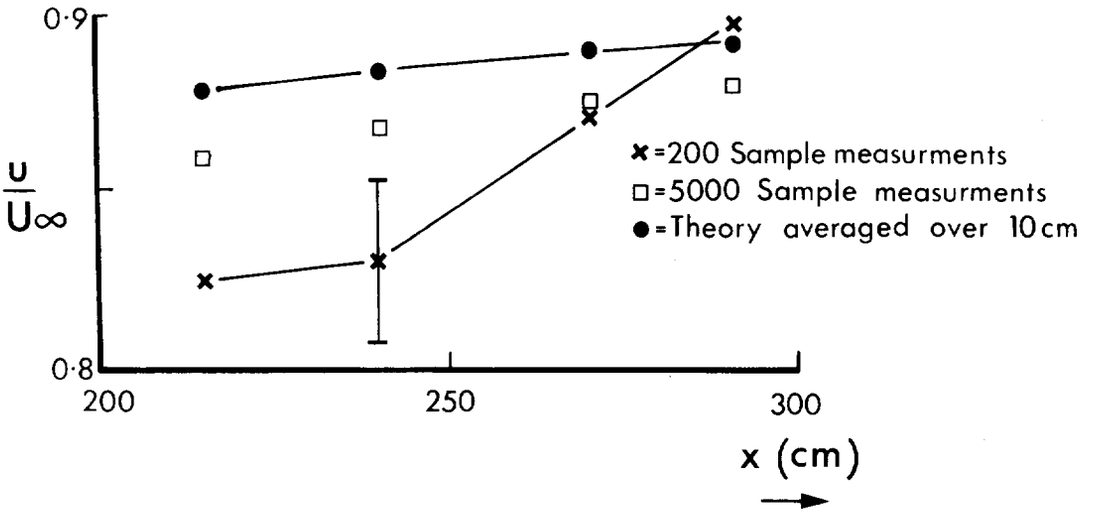

Figure 6. X axis velocity measured by an annular sensor in the wake of a 4.8 cm diameter cylinder.

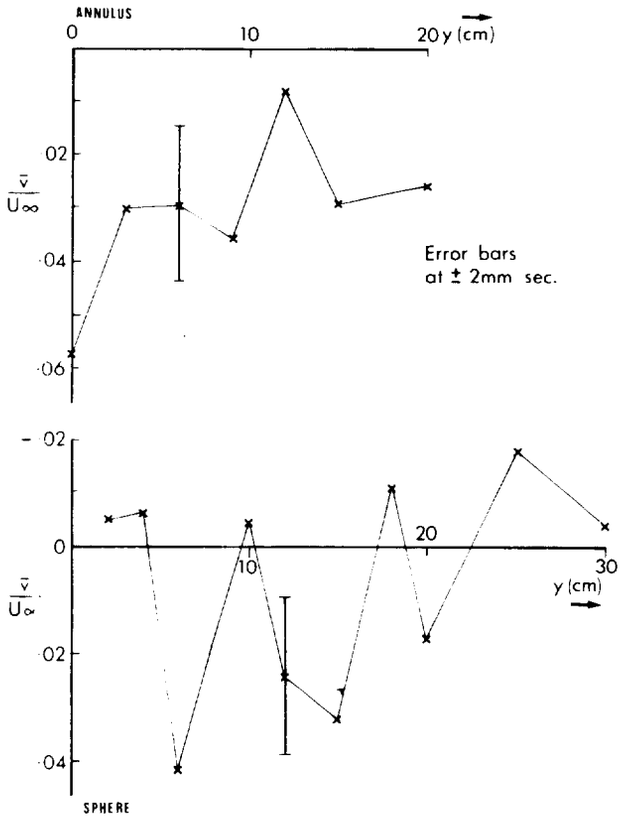

Figure 7. Y axis flow averaged over 20 seconds for a 4.8 cm diameter cylinder.

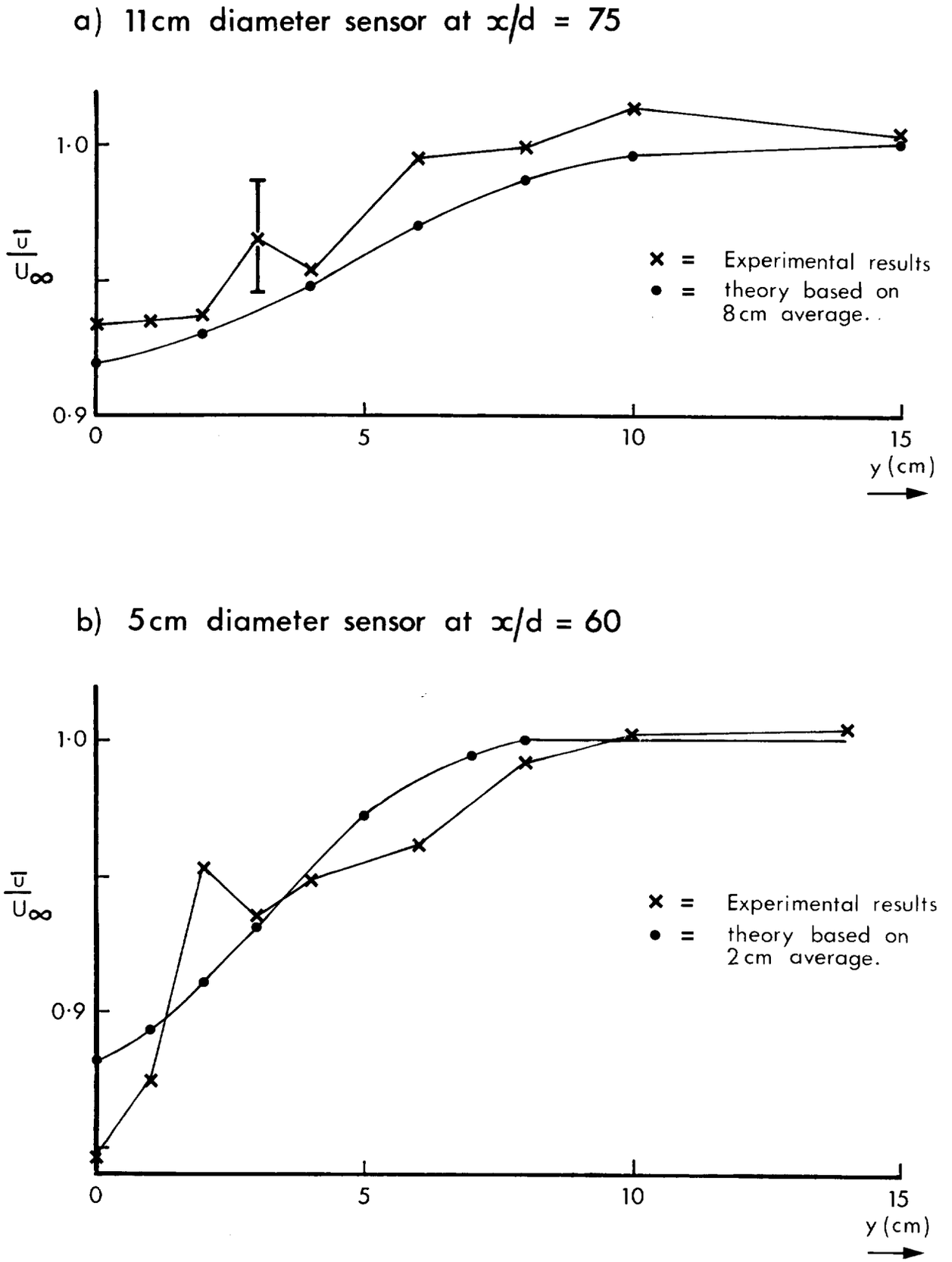

Figure 8. Discus sensor velocity profile across the wake of a 4.8 cm diameter cylinder at $^{x}/_{d}$ = 69.

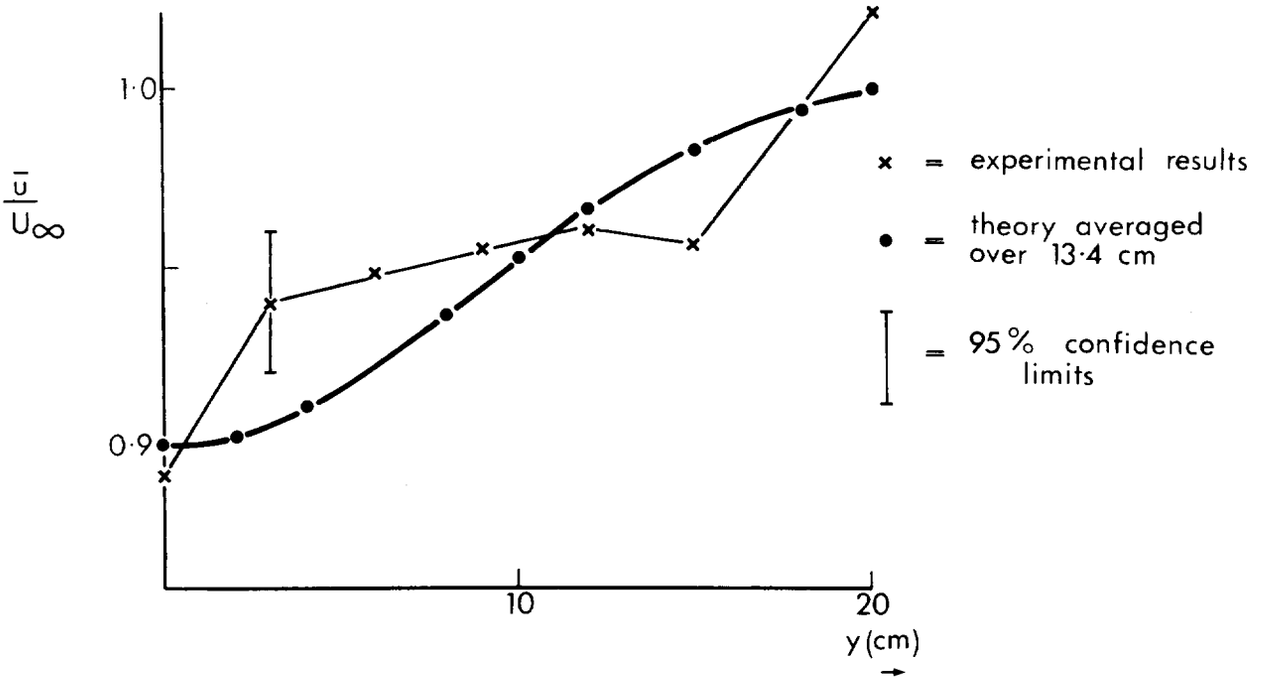

Figure 9. Spherical sensor velocity profile across the wake of a 4.8 cm diameter cylinder at $^{x}/d = 69$.

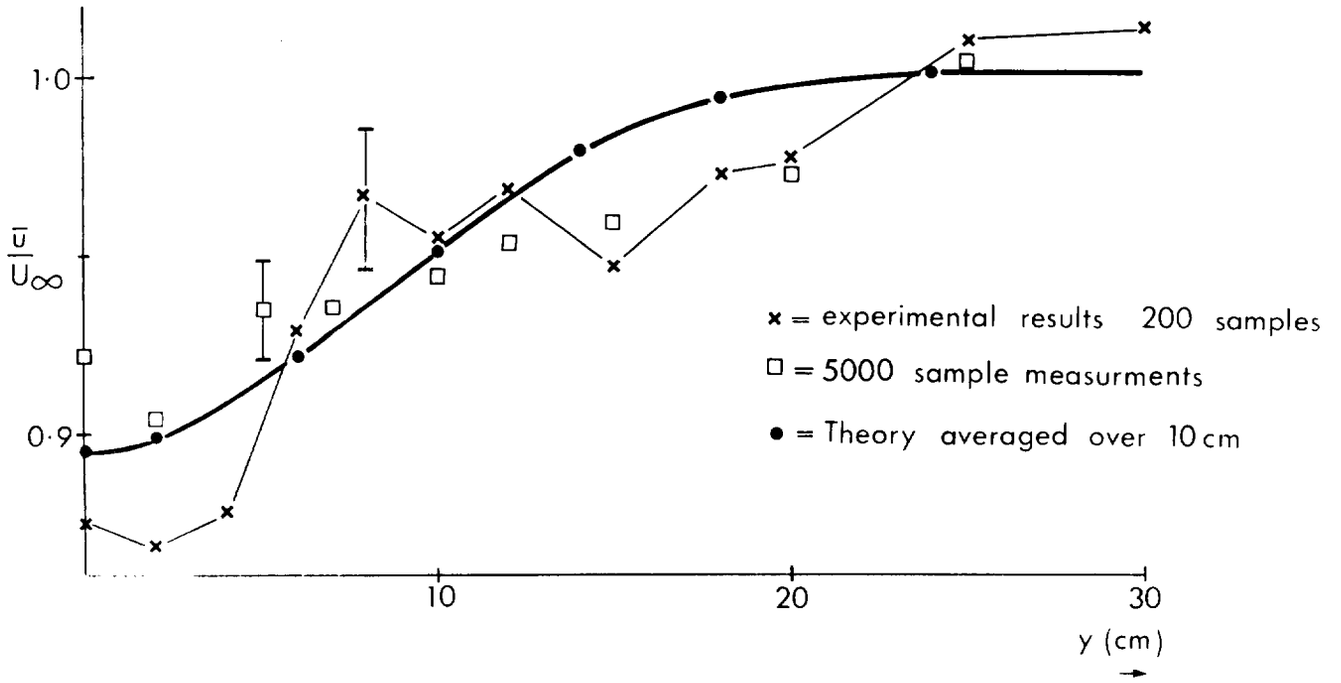

Figure 10. Annular sensor velocity profile across the wake of a 4.8 cm diameter cylinder at $^{x}/d = 69$.

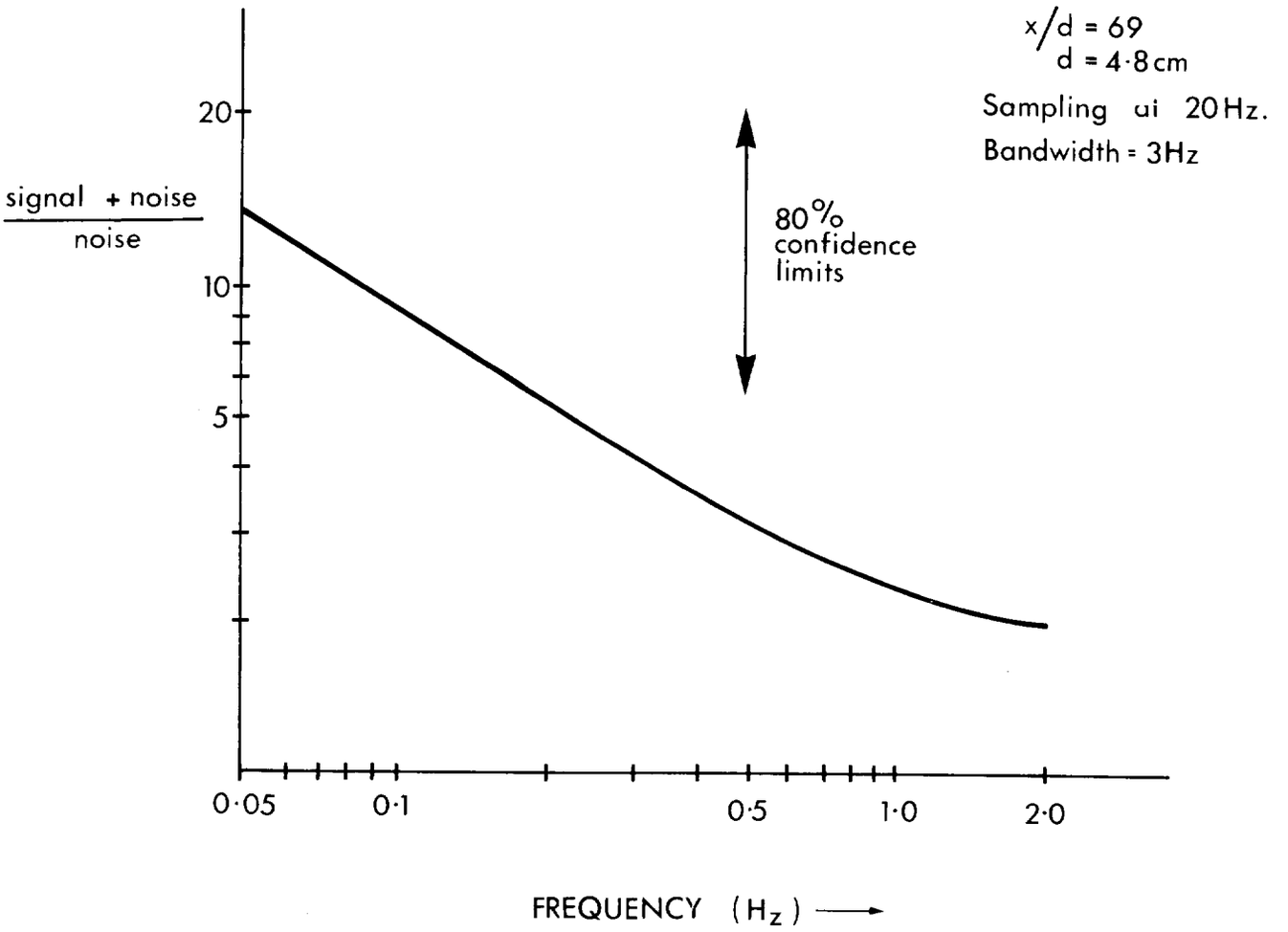

Figure 11. Fluctuation signal + noise to noise ratio for the annular sensor as a function of frequency at 20 cm/sec.

a) 11cm diameter discus at $x/d = 75$

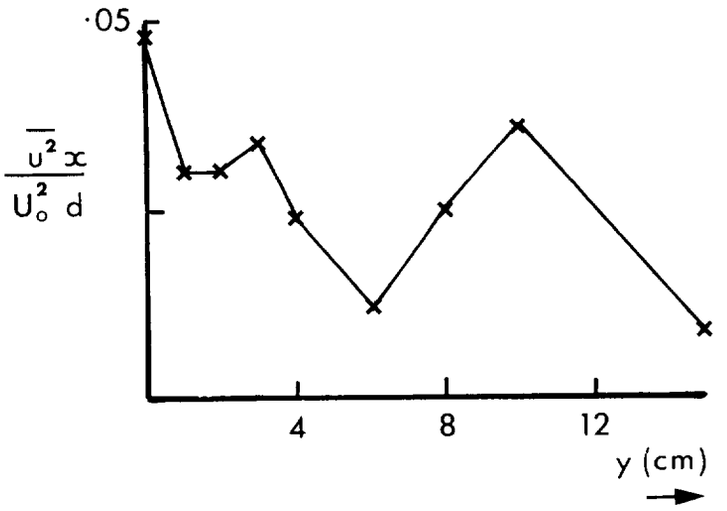

b) 5cm diameter discus at $x/d = 60$

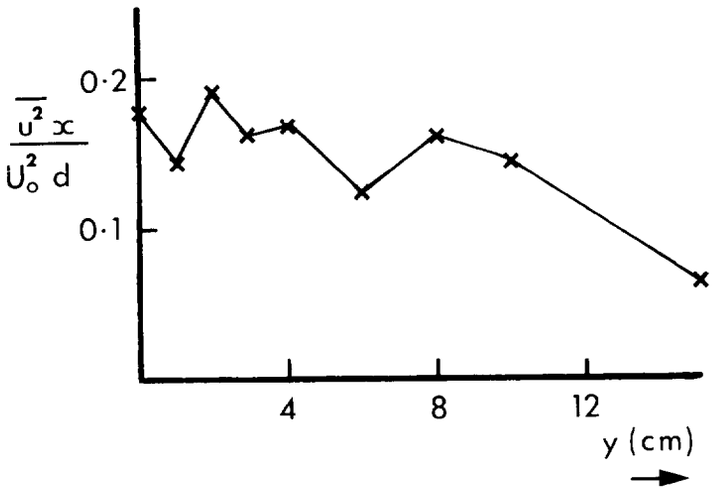

Figure 12. Fluctuation velocity profiles across the wake of a 2 cm cylinder.

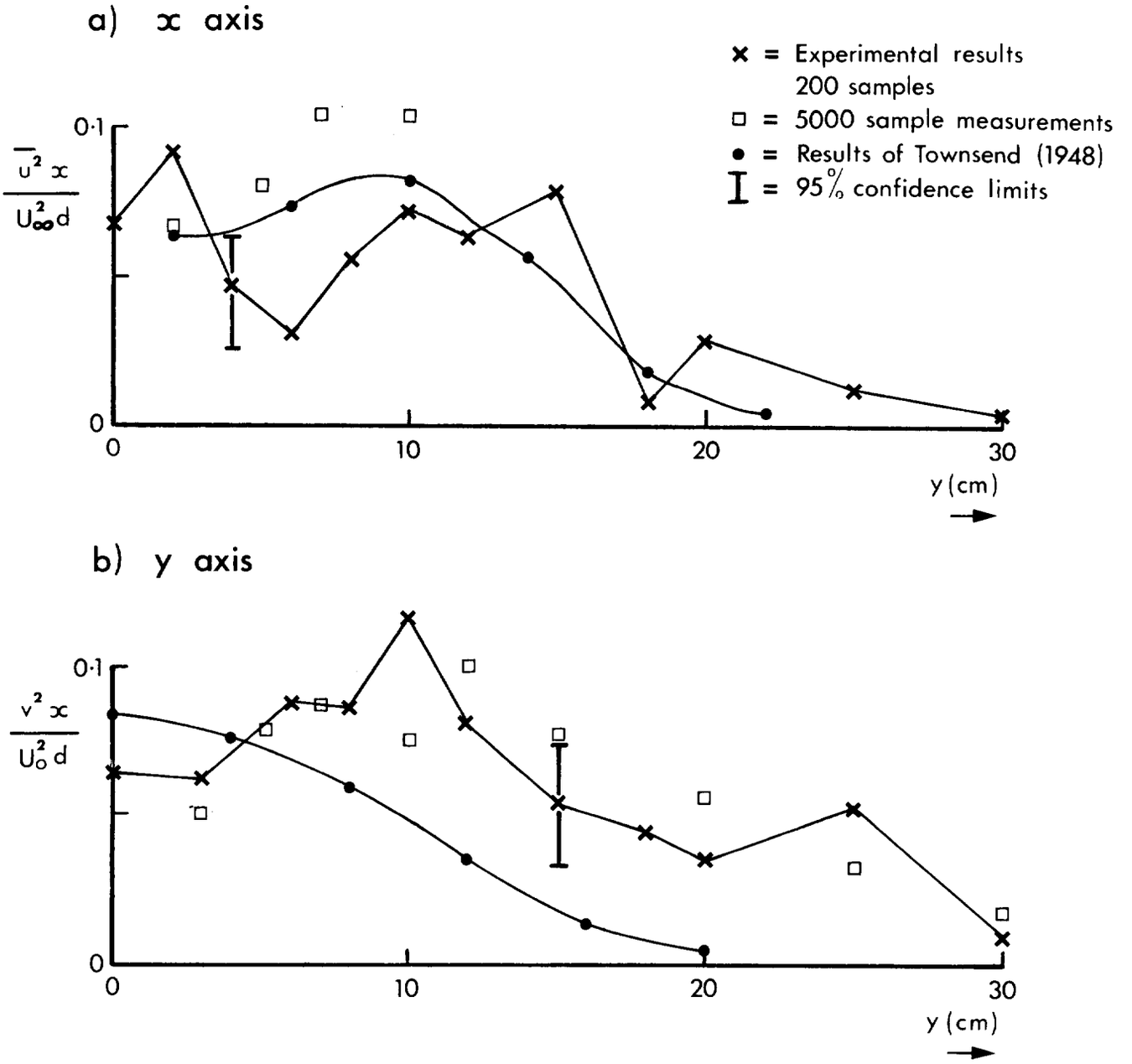

Figure 13. Fluctuation velocity profiles from the annulus at $^x/d$ = 69 for a 4.8 cm diameter cylinder.

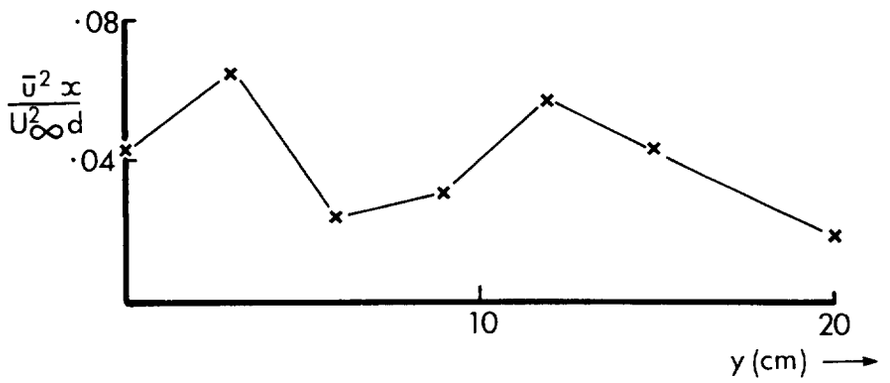

Figure 14. Fluctuation velocity profile measured by the spherical sensor at $^x/d$ = 69 for a 4.8 cm diameter cylinder.

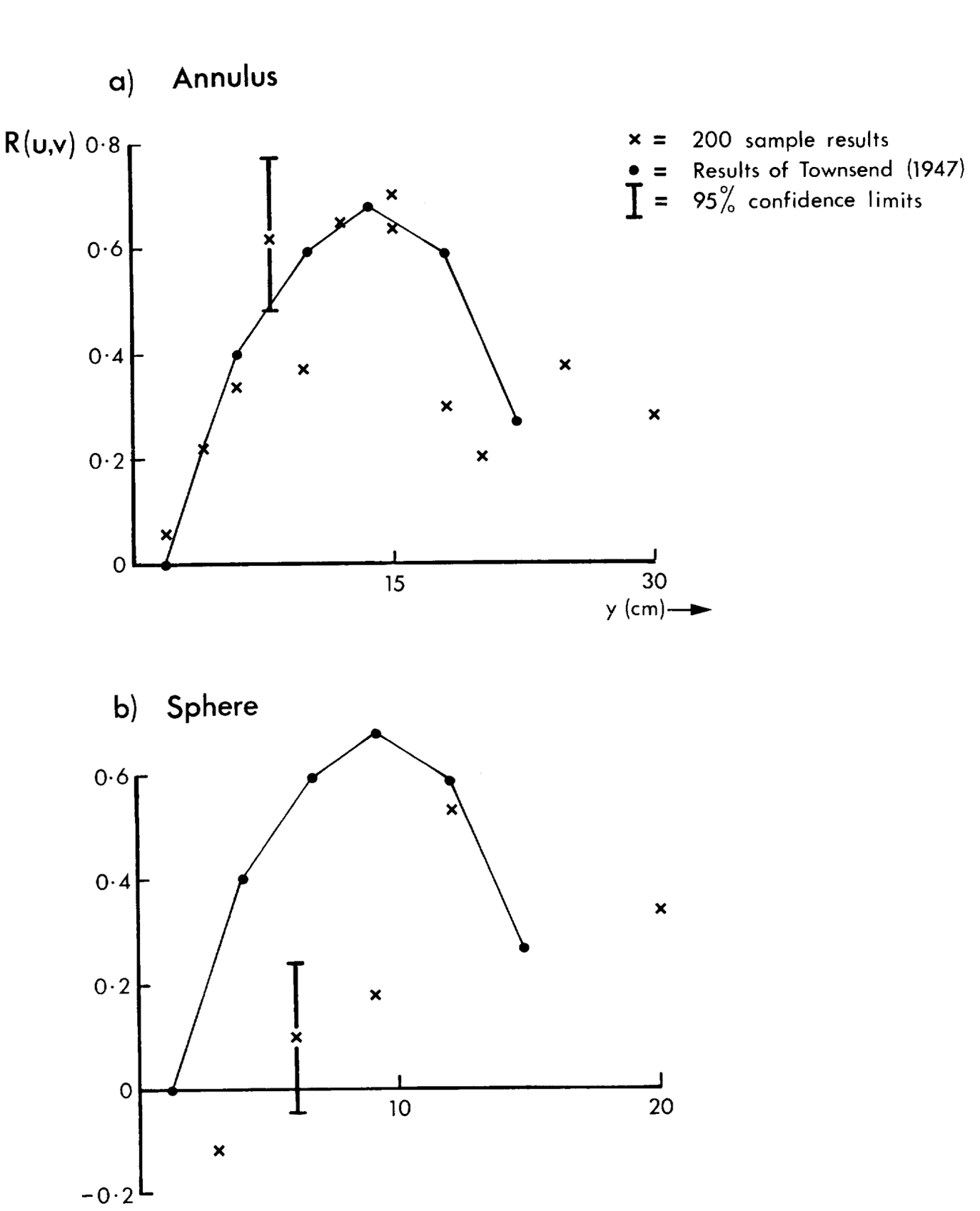

Figure 15. Correlation of u and v velocity fluctuations as a function of y across the wake of a 4.8 cm cylinder at $^{x}/_{d}$ = 69.

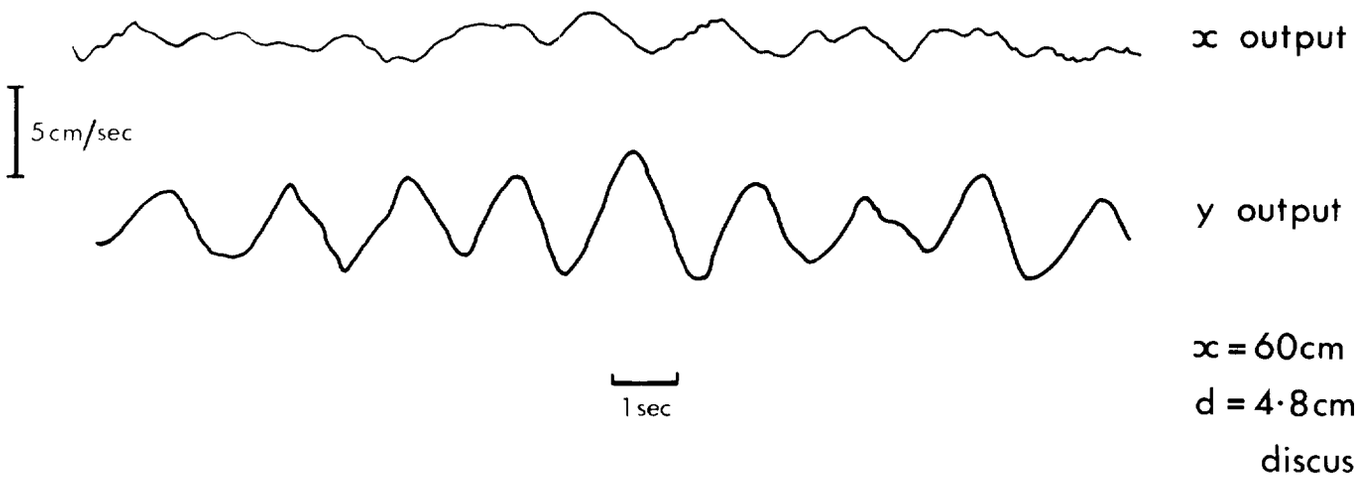

Figure 16(a). UV recorder output from the discus sensor at $^{x}/_{d}$ = 12.5.

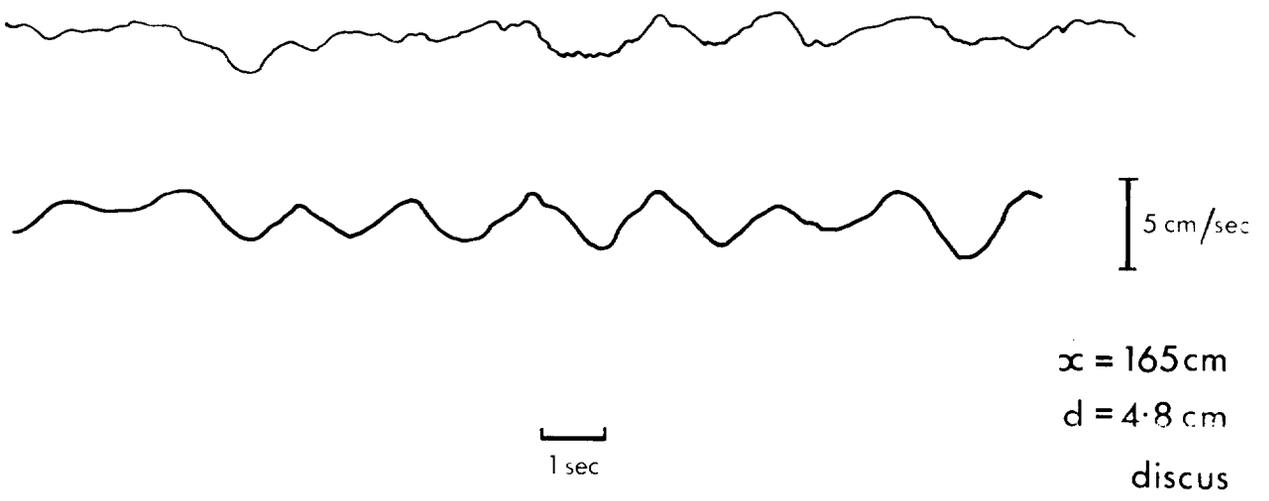

Figure 16(b). $^{x}/_{d}$ = 31.

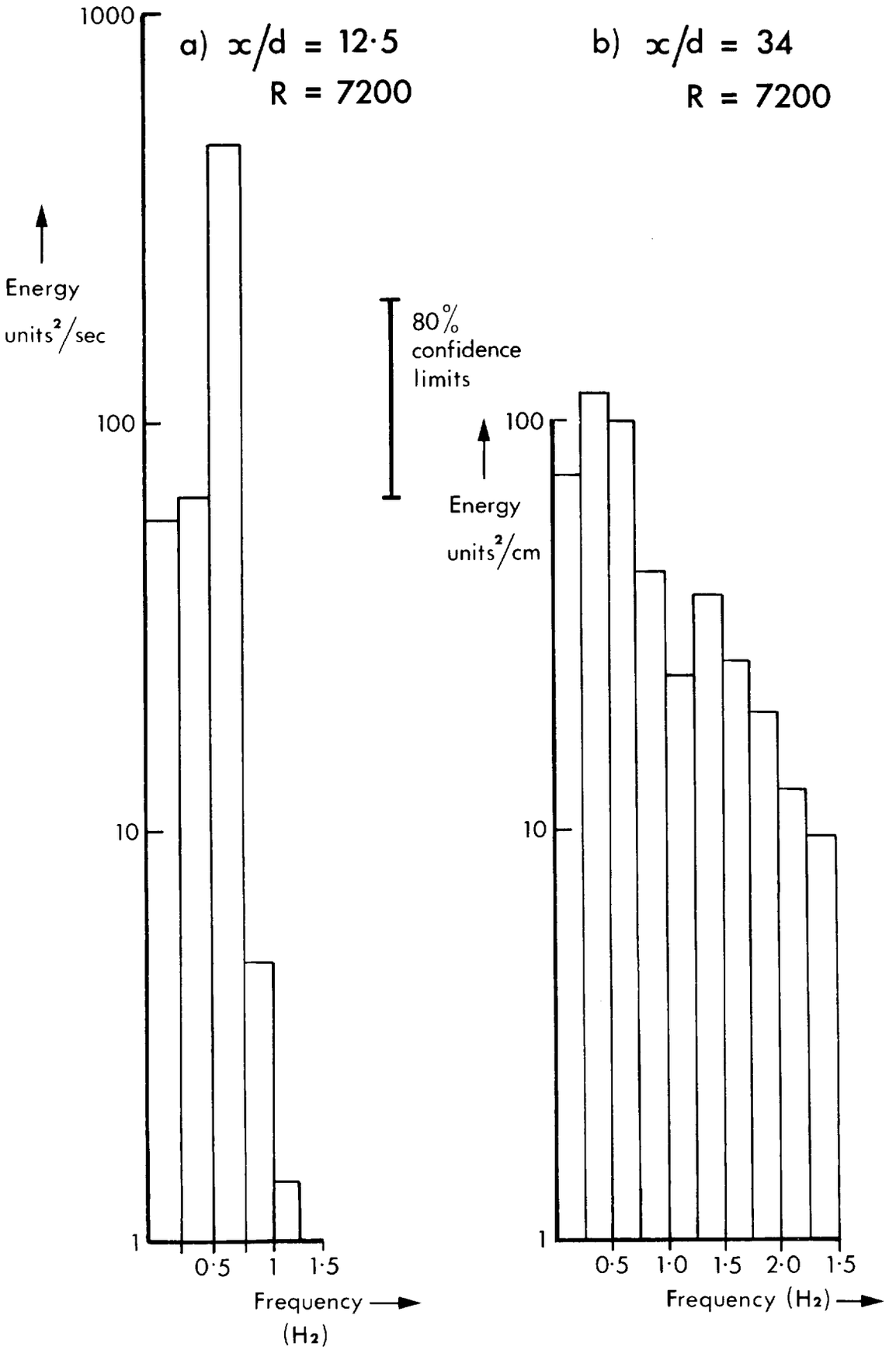

Figure 17. Spectra showing the output of the annular sensor due to vortices near the cylinder, and at the onset of the development into turbulence.

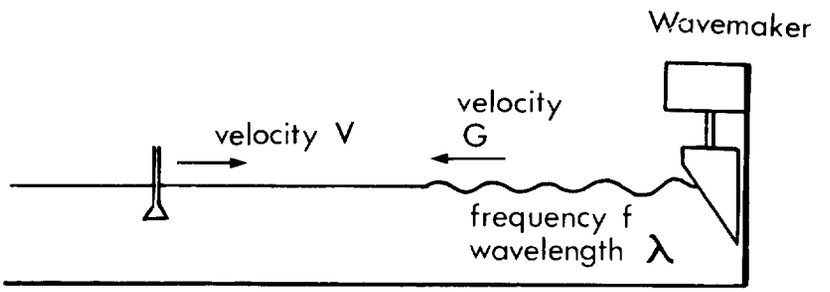

Figure 18. Measurement of spatial response using the wavemaker; diagram of arrangement.

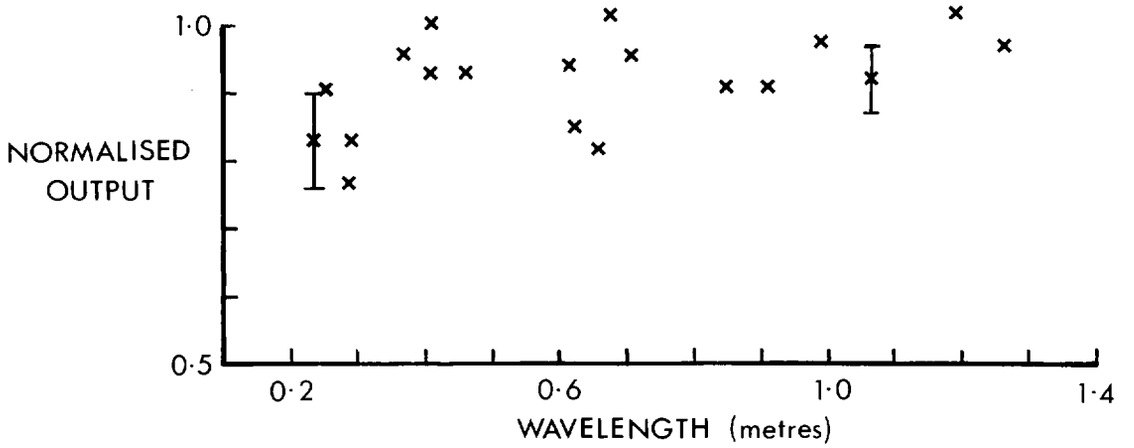

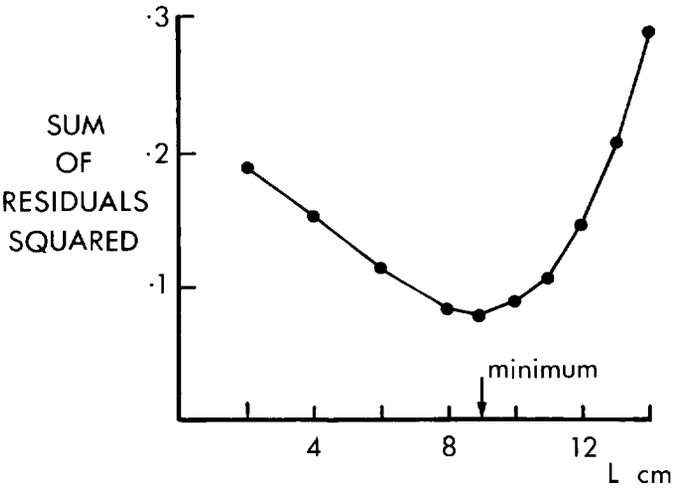

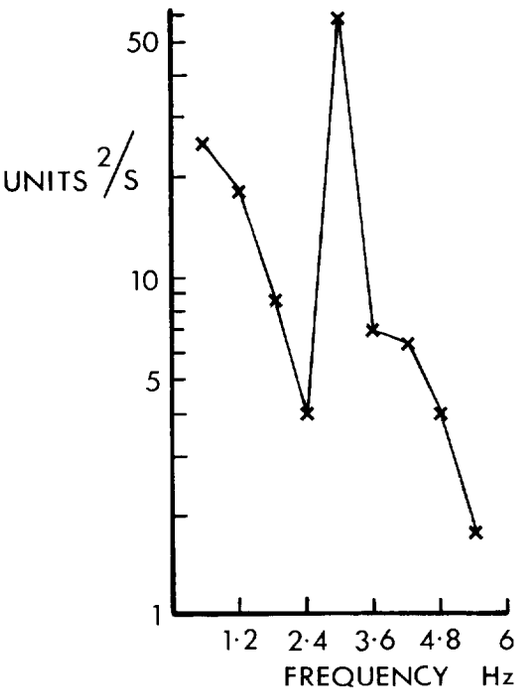

Figure 19. The response of the annulus to waves.
(a) Amplitude response against wavelength.
(b) Residuals of sin $(\pi L/\lambda)/(\pi L/\lambda)$ against L.
(c) Spectrum of sensor output at λ = 26 cm, f wave = 0.5 Hz, speed = 45 cm/s.